A hybrid P1–DP0 diffusion theory for optical imaging

Article *in* Proceedings of SPIE - The International Society for Optical Engineering · February 2009

DOI: 10.1117/12.811356

6 authors, including:

Kai Liu
the ninth hospital Shanghai Jiao Tong Universi…
76 PUBLICATIONS **624** CITATIONS
SEE PROFILE

Jie Tian
Chinese Academy of Sciences
661 PUBLICATIONS **7,099** CITATIONS
SEE PROFILE

Xin Yang
Chinese Academy of Sciences
132 PUBLICATIONS **1,137** CITATIONS
SEE PROFILE

Min Xu
Chinese Academy of Sciences
17 PUBLICATIONS **222** CITATIONS
SEE PROFILE

A hybrid P_1-DP_0 diffusion theory for optical imaging

Kai Liu, Jie Tian, Chenghu Qin, Dan Liu, Xin Yang and Min Xu

Medical Image Processing Group, Institute of Automation, Chinese Academy of Sciences, P. O. Box 2728, Beijing 100190, China

ABSTRACT

In optical imaging, although the standard P_1 diffusion theory is widely used, its angular flux at boundary is discontinuous, and this model is not incapable of exactly modeling light transport in biological tissue with partially-reflective boundary. In this work, we present a hybrid P_1-DP_0 (P_1 spherical harmonics-double DP_0 spherical harmonics) diffusion theory in 3D environment, which effectively interpolates between the P_1 and DP_0 approximation by a space-dependent weight factor $\alpha(r)$ that controls the local angular approximation. Comparing to the P_1 model, the solutions of our model are consistently accurate over a broad range of optical properties. Moreover, with the same *reduced scattering* and *absorption properties*, the hybrid model for high anisotropic scattering which is the common case for mammal tissue is more accurate than the low one. Finally, this theory is validated by Monte Carlo simulations.

Keywords: radiative transfer equation, double spherical harmonics, spherical harmonics, optical imaging, diffusion theory

1. INTRODUCTION

In the biophysics and medicine communities there has been substantial recent interest in such diffusing near-infrared (NIR) light. Optical imaging, which uses low-energy visible or NIR light to probe scattering media, provides new mechanisms for clinical diagnosis of tissue structure and function.[1–7] This is made possible by a spectral window that exists within tissue in about 700-900nm region, in which photon transport is dominated by scattering rather than absorption. Thus, employing the diffusion approximation (P_1 spherical harmonics) to Boltzmann Radiative Transfer Equation (RTE), near-infrared photons diffusing through human tissue is well described.[8] In some new emerging optical imaging modalities such as bioluminescence tomography (BLT) and fluorescence molecular tomography (FMT), the spectrum of the reporters utilized in imaging are not absolutely located in NIR region.[9] As a result, the P_1 diffusion theory is not appropriate and accurate in such applications.

The spherical harmonics (P_N) and double spherical harmonics (DP_N) angular approximations to RTE are well established.[10] In the P_N approximation, the radiance is expanded in Legendre polynomial series. Although more accurate approximations will be achieved if higher order approximation is used, the computation burden becomes extremely high. The desire to more accurately treat the radiance with low order approximations motivated the development of DP_0 diffusion theory. In the DP_N approximation, the radiance is expanded in separate Legendre polynomial expansions over the half ranges $-1 \leq \mu < 0$ and $0 \leq \mu \leq 1$ in one dimension. As a result, the DP_N approximation can more accurately capture the discontinuity in the radiance at interfaces of media and boundaries. However, the DP_N approximation gives less accurate values for the diffusion length than the P_N approximation for optically thick media.[11] Thus, the DP_N approximation may be less accurate for treating light transport through optically thick diffusive media that are not dominated by boundary or media interface effects.

In this paper, to accurately model light transport in biological tissue with low order angular approximations at low cost of time and memory, a hybrid P_1-DP_0 diffusion theory is derived using variational analysis in one dimension. Afterwards, the partially-reflective boundary condition is obtained from RTE boundary condition. Finally, they are transformed from one dimension to three dimension. This hybrid angular approximation contains a space-dependent weight factor $\alpha(r)$ that controls the local angular approximation used at a spatial

Further author information: (Send correspondence to Jie Tian)
Jie Tian: E-mail: tian@ieee.org, Telephone: +86 (10)-82628760

Medical Imaging 2009: Biomedical Applications in Molecular, Structural, and Functional Imaging, edited by Xiaoping P. Hu, Anne V. Clough, Proc. of SPIE Vol. 7262, 72622E · © 2009 SPIE · CCC code: 1605-7422/09/$18 · doi: 10.1117/12.811356

point r: $\alpha(r) = 1$ yields the standard P_1 approximation, $\alpha(r) = 0$ gives the standard DP_0 approximation, and $0 < \alpha(r) < 1$ produces a hybrid P_1-DP_0 angular approximation. The diffusion equation obtained differs from the standard P_1 diffusion equation only in the definition of the diffusion coefficient.

We will introduce the variational derivation of hybrid P_1-DP_0 diffusion theory in detail in section 2. Next, numerical results from several test experiments are presented to demonstrate that significant improvements in accuracy can be obtained using this proposed method with essentially no computational penalty in section 3. The last section goes for discussion and conclusions.

2. METHODS

RTE has successfully been used as a standard model for describing light transport in scattering media. However, providing solutions to the RTE is a major endeavor and remains a challenging task in the fields of biophysics, medicine and radiological sciences. The formulation of the RTE and its boundary condition in three dimension is represented as follows[12,13]:

$$\Big(\hat{s}\cdot\nabla+\mu_s+\mu_a\Big)\psi(r,\hat{s}) = \mu_s\int_{S^2}\psi(r,\hat{s}^{'})\Theta(\hat{s},\hat{s}^{'})\mathrm{d}\hat{s}^{'}+\frac{S(r)}{4\pi} \tag{1}$$

$$\phi(r,\hat{s}) = R(\hat{n}\cdot\hat{s}^{+})\phi(r,\hat{s}^{+}) \quad r\in\partial\Omega \quad \hat{s}\cdot\hat{n}<0 \tag{2}$$

Here $\hat{n}$ is the unit outer normal vector; $\hat{s}$ is the specular reflection of $\hat{s}^{+}$.

We would like to deduce the hybrid P_1-DP_0 model from Eqs. (1) and (2) in one dimension. For the one dimension version of RTE whose range is $0 \le x \le X$, Eq. (1) is degenerated into the following form:

$$\omega\frac{\partial\psi(x,\omega)}{\partial x}+\mu_t\psi(x,\omega) = \mu_s\int_{-1}^{1}\psi(x,\omega^{'})\Theta(\omega,\omega^{'})\mathrm{d}\omega^{'}+\frac{S(x)}{2} \tag{3}$$

For the transport problem Eq. (3), we choose the scalar functional f defined as[14]:

$$f[\phi] = \int_0^X\int_{-1}^{1}\sigma^{*}(x)\phi(x,\omega)\mathrm{d}\omega\mathrm{d}x \tag{4}$$

where $\sigma^{*}(x)$ is a prescribed function. To variationally approximate $f[\phi]$, we use the associated functional $F[\phi,\phi^{*}]$ defined by:

$$\begin{aligned} F[\phi,\phi^{*}] = f[\phi] \quad &- \quad \int_0^X\int_{-1}^{1}\phi^{*}(x,\omega)\Big[\omega\frac{\partial\phi(x,\omega)}{\partial x}+(\mu_s+\mu_a)\phi(x,\omega)\Big]\mathrm{d}\omega\mathrm{d}x \\ &+ \quad \int_0^X\int_{-1}^{1}\phi^{*}(x,\omega)\Big[\mu_s\int_{-1}^{1}\Theta(\omega,\omega^{'})\phi(x,\omega^{'})\mathrm{d}\omega^{'}\Big]\mathrm{d}\omega\mathrm{d}x \\ &+ \quad \int_0^X\frac{1}{2}\phi^{*}(x,\omega)S(x)\mathrm{d}\omega\mathrm{d}x \end{aligned} \tag{5}$$

Before the variational analysis, we should formulate approximate forms for angular flux $\phi(x,\omega)$ and the adjoint angular flux $\phi^{*}(x,\omega)$. The P_1 and DP_0 representation of the angular flux are first given respectively:

$$\phi(x,\omega) = \frac{1}{2}\Phi(x)+\frac{3}{2}\omega J(x) \tag{6}$$

$$\phi(x,\omega) = \frac{1}{2}\Phi(x)+\frac{3}{2}\rho(\omega)J(x) \tag{7}$$

where the functional $\rho(\omega)$ is defined as

$$\rho(\omega) = \begin{cases} +\frac{2}{3} & 0\le\omega\le 1 \\ -\frac{2}{3} & -1\le\omega<0 \end{cases} \tag{8}$$

We note that Eqs. (6) and (7) are similar in form, so we select a weighted hybrid of the P_1 and DP_0 as the function for angular flux which is defined as the hybrid P_1-DP_0 angular approximation:

$$\phi(x,\omega) = \frac{1}{2}\Phi(x) + \frac{3}{2}K(\omega)J(x) \quad -1 \le \omega \le 1 \tag{9}$$

where the functional $K(\omega)$ is defined as

$$K(\omega) = \begin{cases} +\frac{2}{3}[1-\alpha(x)] + \alpha(x)\omega & 0 \le \omega \le 1 \\ -\frac{2}{3}[1-\alpha(x)] + \alpha(x)\omega & -1 \le \omega < 0 \end{cases} \tag{10}$$

Here $0 \le \alpha(x) \le 1$ is a user-prescribed space-dependent weight factor. We define $\alpha(x)$ as:

$$\alpha(x) = 1 - e^{-p(\mu_s+\mu_a)dis(x)} \tag{11}$$

where $dis(x)$ is the distance to the nearest boundary at a spatial point x and parameter p satisfies $10^{-4} \le p \le 10^{-3}$. For $\alpha(x) = 1$, Eq. (9) is the P_1 angular approximation, and $\alpha(x) = 0$ the DP_0 angular approximation. Setting $0 < \alpha(x) < 1$ yields a weighted hybrid of the P_1 and DP_0 angular approximation. For the adjoint trial function, we use a similar form:

$$\phi^*(x,\omega) = \frac{1}{2}\Phi^*(x) + \frac{3}{2}K(\omega)J^*(x) \quad -1 \le \omega \le 1 \tag{12}$$

In the variational analysis, we substitute the approximate forms Eqs. (9) and (12) into Eq. (5) and integrate angular to reduce the following form:[15,16]

$$\begin{aligned} F[\Phi(x), J(x), \Phi^*(x), J^*(x)] &= \int_0^X \sigma^*(x)\Phi(x)\mathrm{dx} \\ &- \frac{1}{2}\int_0^X \Phi^*(x)\Big[\frac{dJ(x)}{dx} + \mu_a\Phi(x) - S(x)\Big]\mathrm{dx} \\ &- \frac{3}{2}\int_0^X J^*(x)\Big[\frac{1}{3}\frac{d\Phi(x)}{dx} + \mu_a^{'}J(x)\Big]\mathrm{dx} \end{aligned} \tag{13}$$

where

$$\mu_a^{'} = \Big[1 + \frac{1}{3}(1-\alpha(x))^2\Big](\mu_a + \mu_s) - g\mu_s - \Sigma(x) \tag{14}$$

and

$$\Sigma(x) = \frac{3}{2}\sum_{l=3,l:odd}^{\infty}\frac{2l+1}{2}g^l\mu_s\Big[\int_{-1}^{1}P_l(\omega)K(x,\omega)\mathrm{d}\omega\Big]^2 \tag{15}$$

Note that the P_l are the Legendre polynomials, and the quantity $\Sigma(x)$ in Eq. (14) is zero only for $\alpha(x) = 1$, i.e. only for the P_1 angular approximation.

Calculate the first variation δF of Eq. (13), with respect to independent variations of the unknown functions $\delta\Phi(x)$, $\delta J(x)$, $\delta\Phi^*(x)$, $\delta^* J(x)$, and set the results to zero, we will obtain the hybrid P_1-DP_0 equations

$$\frac{dJ(x)}{dx} + \mu_a\Phi(x) = S(x) \quad 0 < x < X, \tag{16}$$

and

$$\frac{1}{3}\frac{d\Phi(x)}{dx} + \mu_a^{'}J(x) = 0 \quad 0 < x < X \tag{17}$$

Eliminating $J(x)$, Eqs. (16) and (17) can be deduced into a diffusion theory:

$$-\frac{d}{dx}\Upsilon(x)\frac{d}{dx}\Phi(x) + \mu_a\Phi(x) = S(x) \quad 0 < x < X \tag{18}$$

here the diffusion coefficient is given by $\Upsilon(x) = 1/[3\mu_a^{'}(x)]$. In the formal derivation of the three dimension equations, one simply replaces the diffusion operator by its three dimension counterpart. That is, we replace:

$$\frac{d}{dx}\Upsilon(x)\frac{d}{dx}\Phi(x) \quad by \quad \nabla\Upsilon(r)\cdot\nabla\Phi(r) \tag{19}$$

Thus, Eq. (18) becomes:

$$-\nabla\Upsilon(r)\cdot\nabla\Phi(r) + \mu_a\Phi(r) = S(r) \quad r \in \Omega \tag{20}$$

Integrate the Eq. (2) on the 4π solid angular, we obtain the partially-reflective boundary condition:

$$\Phi(r) + 2\Upsilon(r)A(r;n,n^{'})\Big(\hat{n}\cdot\nabla\Phi(r)\Big) = 0 \quad r \in \partial\Omega \quad where \quad A(r;n,n^{'}) = \frac{1+R_{eff}(r)}{1-R_{ff}(r)} \tag{21}$$

In this study, the surrounding medium is air, so $n^{'}$ is approximately 1, and $R_{eff}(r)$ is the effective reflection coefficient, which can be calculated by[18]:

$$R_{eff}(r) \approx -1.4399n^{-2} + 0.7099n^{-1} + 0.6681 + 0.0636n \tag{22}$$

Therefore, the output flux on the boundary captured by a highly sensitive CCD camera is given by

$$Q(r) = -\Upsilon(r)\frac{\partial\Phi(r)}{\partial n} = \frac{\Phi(r)}{2A(r;n,n^{'})} \quad (r \in \partial\Omega) \tag{23}$$

3. FINITE ELEMENT FORMULATION OF THE HYBRID DIFFUSION THEORY

Using the finite element method,[17] Eqs. (20) and (21) are deduced into its equivalent variation formulation in which $\Phi(r) \in H_0^1(\Omega)$ can be satisfied such that[18, 20]:

$$\int_\Omega \Big(\Upsilon(r)\nabla\Phi(r)\nabla\Psi(r) + \mu_a(r)\Phi(r)\Psi(r)\Big)\mathrm{d}r + \int_{\partial\Omega}\frac{\Phi(r)\Psi(r)}{2A(r;n,n^{'})}\mathrm{d}r = \int_\Omega S(r)\Psi(r)\mathrm{d}r \quad (\forall\Psi(r) \in H_0^1(\Omega)) \tag{24}$$

To solve the Eq. (24) numerically, the infinite dimensional function space Ω should be substituted by a finite dimensional approximation Ω^h consisting of N_p vertex nodes and N_e elements (here we use tetrahedral), denoted as Ω^l $(l = 1, 2, ..., N_e)$, such that $\Omega^h = \bigcup_{l=1}^{N_e}\Omega^l$. Hence Ω is partitioned into continuous piecewise polynomial functions[18]:

$$\Phi(r) \approx \Phi^h(r) = \sum_{k=1}^{N_p}\phi_k\varphi_k(r) \ when \ r \in \Omega^h(r) \tag{25}$$

where ϕ_k is the value of $\Omega(r)$ on the $k-th$ node, and $\varphi_k(r)$ the nodal basis function within the elements Ω^l. Similarly, the source function $S(r)$ is approximated as[18]:

$$S(r) \approx S^h(r) = \sum_{k=1}^{N_p}s_k\varphi_k(r) \ when \ r \in \Omega^h(r) \tag{26}$$

here s_k is the value of $S(r)$ on the $k-th$ node. We choose the same nodal basis functions as $\Phi(r)$, which are C^0 and can be more accurate than the element basis functions.[18]

Substituting Eqs. (25) and (26) into Eq. (24), and using the nodal basis functions $\varphi_k(r)$ as the basis functions, we obtain the matrix equation as follows[19]:

$$(K + C + B)\Phi = M\Phi = FS = b \tag{27}$$

where the components of the matrices are given by[21]

$$\begin{cases} k_{ij} = \int_{\Omega} \Upsilon(r)\nabla\varphi_i(r)\nabla\varphi_j(r)\mathrm{dr} \\ c_{ij} = \int_{\Omega} \mu_a(r)\varphi_i(r)\varphi_j(r)\mathrm{dr} \\ b_{ij} = \int_{\partial\Omega} \dfrac{\varphi_i(r)\varphi_j(r)}{2A(r;n,n')}\mathrm{dr} \\ f_{ij} = \int_{\Omega} \varphi_i(r)\varphi_j(r)\mathrm{dr} \end{cases} \tag{28}$$

It is observed that the hybrid diffusion theory obtained from variational analysis differs from the standard P_1 diffusion theory only in the value of the diffusion coefficient. Therefore, it is easily incorporated into a standard diffusion solver. Here, the problem in Eq.(27) will be solved by a finite-element-based solver which we have developed previously.[22] Since there are about only 1% non-zero in matrices in Eq.(27), the matrices are all sparse. It is not only very memory-efficient, but computation-efficient.

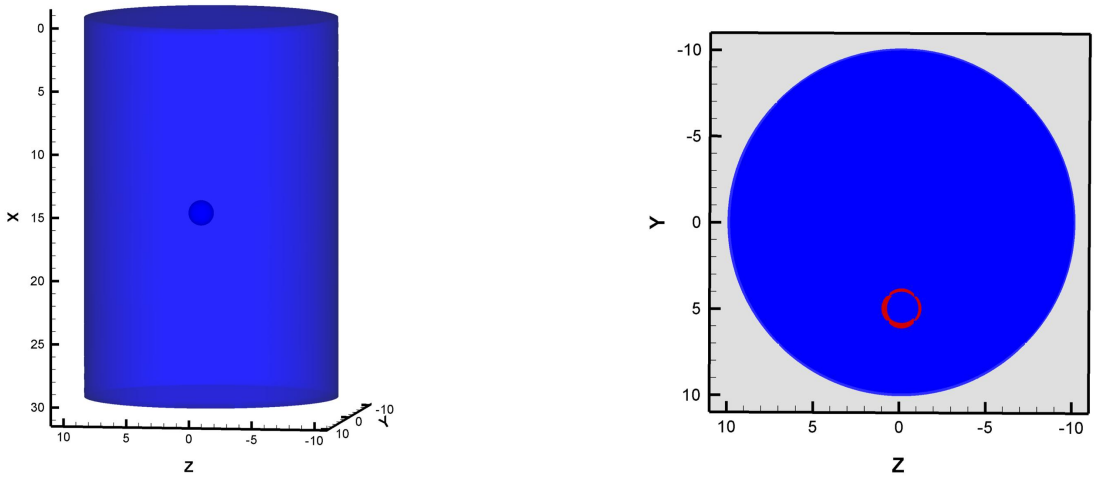

(a) (b)

Figure 1. The phantom used in MOSE simulation and numerical experiments. (a) The profile in three dimension. The sphere in the cylinder is the source; (b) A truncation surface at x=15mm. The virtual detectors used in experiments are located on the boundary of this circle.

4. NUMERICAL EXPERIMENTS AND RESULTS

4.1. Simulating experiment results using Monte Carlo method

We use MOSE (a Monte Carlo based method) to generate the exact results for comparison,[23] which is a gold standard for this partial differential problem. The grids used in MOSE are structured by surface triangles for each region. In our experiments, a cylinder tissue-like phantom with $30mm$ height and $10mm$ radius is utilized as shown in Fig. 1. A spherical bioluminescent source with the location of $(15, 5, 0)$, $1mm$ radius and $238pW/mm^3$ power density is embedded in the phantom. Here the grids are discretized into 39570 triangular elements with the maximum diameter of 0.8mm. A total of 158536 virtual detectors are allocated on the surface of phantom to record output flux. The source is assumed to obey uniform distribution and sampled to 10^6 photon packets. Three simulation experiments are performed in advance for different *optical albedos* (*i.e.* μ_s'/μ_a): 400, 40 and 5, respectively, and the output flux detected on whole surface of the phantom is depicted in Fig. 2.

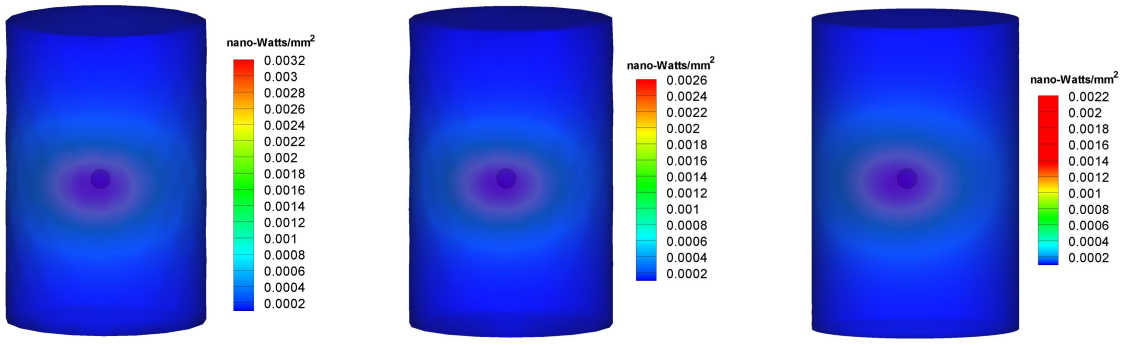

(a) (b) (c)

Figure 2. Output flux detected on whole surface of the phantom. (a) Measurements with optical properties: $\mu_s^{'} = 0.4mm^{-1}$, $\mu_a = 0.001mm^{-1}$. (b) Measurements with optical properties: $\mu_s^{'} = 0.4mm^{-1}$, $\mu_a = 0.01mm^{-1}$. (c) Measurements with optical properties: $\mu_s^{'} = 0.2mm^{-1}$, $\mu_a = 0.04mm^{-1}$.

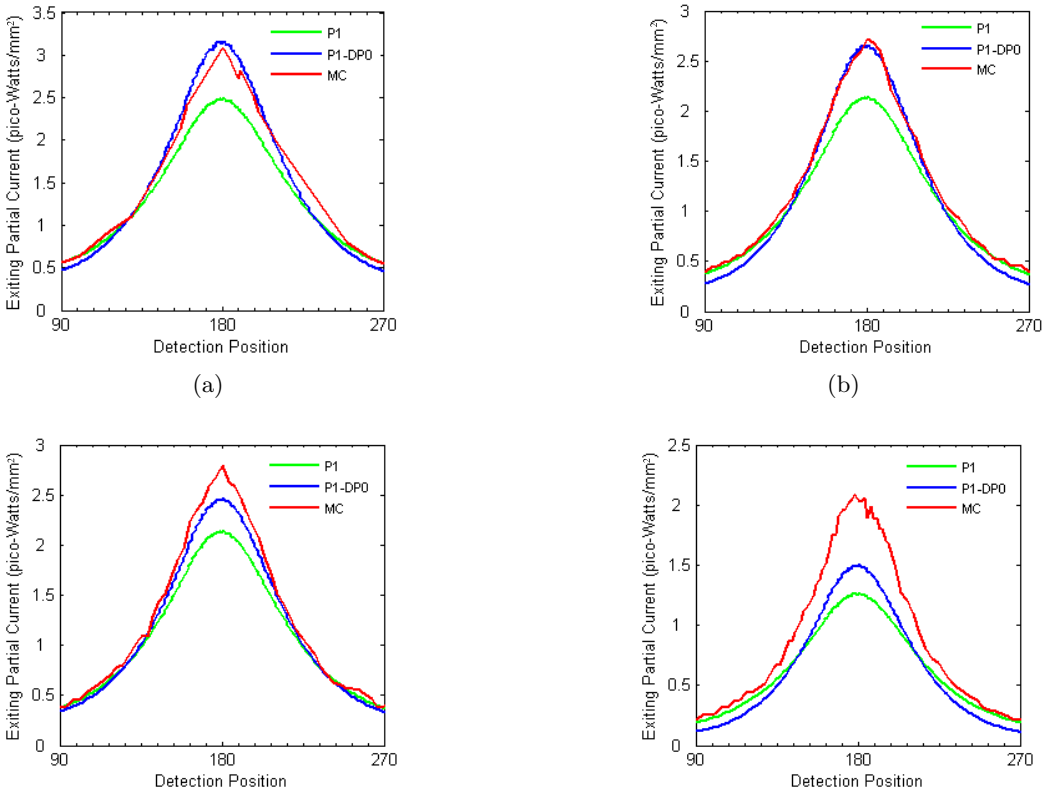

(a) (b) (c) (d)

Figure 3. Comparing output flux of P_1, P_1-DP_0 and MOSE in region of interest along detection circle at $x = 15mm$. (a) Numerical experiment with optical properties: $\mu_s = 4.0mm^{-1}$, $\mu_a = 0.001mm^{-1}$, $g = 0.9$; (b) Numerical experiment with optical properties: $\mu_s = 4.0mm^{-1}$, $\mu_a = 0.01mm^{-1}$, $g = 0.9$; (c) Numerical experiment with optical properties: $\mu_s = 0.8mm^{-1}$, $\mu_a = 0.01mm^{-1}$, $g = 0.5$; and (d) Numerical experiment with optical properties: $\mu_s = 2.0mm^{-1}$, $\mu_a = 0.04mm^{-1}$, $g = 0.9$.

4.2. Comparison between the hybrid P_1-DP_0 and standard P_1 diffusion theory

In order to verify the proposed theory, four comparison experiments with different optical properties are carried on. Fig.3 depicts the output flux for the results of MOSE, P_1 and P_1-DP_0 on the detector circle at $x = 15mm$. It is shown that P_1-DP_0 theory agrees well with the MOSE simulations with the relative errors about 1.400%, 4.627%, 6.567% and 27.035% respectively. In contrast, the relative errors between the solutions of the P_1 and MOSE are 9.421%,11.435%, 12.816% and 27.552%.

The numerical experiments show that the P_1-DP_0 theory agrees consistently better with MOSE than the standard P_1. The cases of high *optical albedos* is better than the low ones. Even in the case of *optical albedo*=5, the performance of hybrid theory is better than the standard P_1 theory, especially around the region of the peak output flux. Furthermore, with the same *optical albedo* (40), the solutions for the high forward-peaked case ($g = 0.9$, Fig. 3(c)) matches better with MOSE than that of the low one ($g = 0.5$, Fig. 3(b)). The parameter p is set 0.33×10^{-3} for the first three cases, and 1×10^{-4} for the last case. In addition, since the hybrid diffusion theory obtained from our variational analysis differs from the standard P_1 diffusion theory only in the value of the diffusion coefficient, it requires essentially the same computational effort as standard P_1 theory. In the four experiments, the consuming time of hybrid theory is almost identical with P_1 theory.

5. DISCUSSION AND CONCLUSIONS

In the biophysics and medicine especially in the emerging molecular imaging, although the P_1 diffusion theory is widely used, it gives a relatively poor approximation for angular flux and output flux. However, the DP_0 approximation can exactly satisfy the boundary conditions in optical imaging. As a result, to the best of Our knowledge, for the first time we construct the DP_0 approximation coupled with the P_1 approximation in optical imaging to more accurately treat the partial reflective boundary, and thus more accurately model light transport in biological tissue with almost the same computational cost as the standard P_1 approximation. This hybrid angular approximation contains a user-prescribed space-dependent weight factor $\alpha(r)$ that controls the local angular approximation used at a given spatial point r. $\alpha(r) = 1$ yields the standard P_1 approximation, $\alpha(r) = 0$ gives the standard DP_0 approximation, and $0 < \alpha(r) < 1$ produces a hybrid P_1-DP_0 approximation. We propose a simple but effective functional form for the weight factor $\alpha(r)$ that accomplishes this desired behavior and that avoids the need for users to specify the value.

In conclusion, we present here a hybrid P_1-DP_0 diffusion theory for modeling light transport in biological tissue. Our method requires essentially the same computational effort as standard P_1 diffusion theory. Using this method, the approximation results are highly improved in contrast with P_1, and it is verified the effectiveness and potential for the optical imaging.

ACKNOWLEDGMENTS

This work is supported by the Project for the National Basic Research Program of China (973) under Grant No.2006CB705700, Program Changjiang Scholars and Innovative Research Team in University (PCSIRT) under Grant No.IRT0645, CAS Hundred Talents Program, CAS scientific research equipment develop program (YZ0642,YZ200766), the Joint Research Fund for Overseas Chinese Young Scholars under Grant No.30528027, the National Natural Science Foundation of China under Grant Nos.30672690, 30600151, 90209008, 60532050, 60621001, 30873462, Beijing Natural Science Fund under Grant No.4071003.

REFERENCES

1. A. Yodh and B. Chance, "Spectroscopy and imaging with diffusing light," *Physics Today* **48**, pp. 34-40, 1995.
2. A. P. Gibson, J. C. Hebden, and S. R. Arridge, "Recent advances in diffuse optical imaging," *Phys. Med. Biol.* **50**, pp. R1-R43, 2005.
3. A. H. Hielscher, "Optical tomographic imaging of small animals," *Curr. Opin. Biotechnol.* **16**, pp. 79-88, 2005.

4. V. Ntziachristos, J. Ripoll, L.V. Wang, and R. Weisslder,"Looking and listening to light: the evolution of whole body photonic imaging," *Nature Biotechnology* **23,** 313-320, 2005.
5. R. Weissleder, M.J. Pittet, "Imaging in the era of molecular oncology," *Nature* **452,** 580-589, 2008.
6. J. Tian, J. Bai, X.-P. Yan, S.-L. Bao, Y.-H., Liang W. Li and X. Yang, "Multimodality molecular imaging," *IEEE EMB Magazine* **27,** 48-57 2008.
7. J.K. Willmann, N. van Bruggen, L.M. Dinkelborg and S.S. Gambhir, "Molecular imaging in drug development," *Nature* **7,** 591-607, 2008.
8. L. V. Wang, H. Wu, *Biomedical Optics*, Wiley-Interscience, New York, 2007.
9. B. W. Rice, M. D. Cable, and M. B. Nelson, "In vivo imaging of light-emitting probes," *Journal of Biomedical Optics* **6**, pp. 432-440, 2001.
10. G. I. Bell and S. Glasstone, *Nuclear Reactor Threory*, Robert E. Krieger Publishing Co., New York, 1970.
11. B. Davison, *Neutron Transport Theory*, Oxford University Press, London, 1957.
12. A. D. Klose, U. Netzb, J. Beuthanb, A. H. Hielscher, "Optical tomography using the time-independent equation of radiative transfer – Part 1: forward model," *Journal of Quantitative Spectroscopy & Radiative Transfer* **72**, 691-713, 2002.
13. A. D. Klose, E. W. Larsen, "Light transport in biological tissue based on the simplified spherical harmonics equations," *Journal of Computational Physics* **220**, 441-470, 2006.
14. P. S. Brantley, "A mixed P_1-DP_0 diffusion theory for planar geometry," *Annals of Nuclear Energy* **32**, 1525-1545, 2005.
15. E. W. Larsen, J. E. Morel, and J. M. McGhee, "Asymptotic derivation of the multigroup P1 and simplified PN equations with anisotropic scattering," *Nucl. Sci. Eng.* **123**, pp. 328-342, 1996.
16. E. W. Larsen. G. Thömmes, A. Klar, M. Seaïd, and T. Götz, "Simplified P_0 approximations to the equations of radiative heat transfer and applications", *Journal of Computational Physics* **183**, pp. 652C675, 2002.
17. S. C. Brenner, L. C. Scott,*The Mathematical Theory of Finite Element Methods*, Springer-Verlag, New York, 1994.
18. W. Cong, G. Wang, D. Kumar, Y. Liu, M. Jiang, L. Wang, E. Hoffman, G. McLennan, P. McCray, J. Zabner, and A. Cong, "Practical reconstruction method for bioluminescence tomography," *Opt. Express* **13,** 6756-6771, 2005.
19. G. Wang, H. Shen, W. Cong, S. Zhao, G. Wei, "Temperature-modulated bioluminescence tomography," *Opt. Express* **14**, pp. 7852-7871, 2006.
20. Y. Lv, J. Tian, W. Cong, J. Luo, W. Yang, H. Li, "A multilevel adaptive finite element algorithm for bioluminescence tomography," *Opt. Express,* **14**, pp. 8211-8223, 2006.
21. S. R. Arridge, M. Schweiger, M. Hiraoka, and D. T. Delpy, "A finite element approach for modeling photon transport in tissue," *Medical Physics,* **20**, pp.299-309, 1993.
22. Y. Lv, J. Tian, H. Li, J. Luo, W. Cong, G. Wang and D. Kumar, "Modeling the forward problem based on the adaptive FEMs framework in bioluminescence tomography," in *Developments in X-Ray Tomography V*, U. Bonse, ed., **6318**, pp. 63180I.1-63180I.8, SPIE, 2006.
23. H. Li, J. Tian, F. Zhu , W. Cong, L. Wang, E. Hoffman, G. Wang, "A mouse optical simulation environment (MOSE) to investigate bioluminescent phenomena in the living mouse with the Monte Carlo Method," *Acad. Radiol.* **11**, pp. 1029-1038, 2004.